CrossMark

The mechanical design of a hybrid intelligent hinge with shape memory polymer and spring sheet

Changguo Wang [a, b, *], Yafei Wang [a]

[a] Center for Composite Materials, Harbin Institute of Technology, Harbin 150001, PR China
[b] National Key Laboratory of Science and Technology on Advanced Composites in Special Environments, Harbin Institute of Technology, Harbin 150080, PR China

ARTICLE INFO

ABSTRACT

In this paper a concept of hybrid intelligent hinge is proposed to improve the deployment efficiency of the intelligent hinge. The hybrid intelligent hinge system consists of two shape memory polymer thin shells and one spring sheet based on the win-win considerations. The bending moment of hybrid intelligent hinge system is predicted theoretically. The bending process of hybrid intelligent hinge system is simulated and divided into three typical stages which correspond to three different bending mechanisms. The bending experiments are then performed to verify the recovery ability of hybrid intelligent hinge system. A parametric analysis is then carried out to obtain the bending rules of hybrid intelligent hinge system, based on which the hybrid intelligent hinge system with a variable range of recovery moment can be designed. The results obtained in this paper give a guide to design a promising intelligent hinge of deployable structures.

© 2017 Elsevier Ltd. All rights reserved.

1. Introduction

The intelligent hinge using elastic memory composite (EMC) was first proposed by the company of Composite Technology Development (CTD). Then the application of the EMC hinge was developed in the field of aerospace industry [1]. In the mission of TacSat-2, the EMC hinge was applied in its one wing [2]. Then with the support of DR Technology, considering the low cost, CTD applied the intelligent hinge in the deployable solar array of TacSat-4 [3]. Compared to traditional mechanical actuators, intelligent hinge is simple and lightweight, while it decreases the impact from the deployable process [4]. However, the application scope of intelligent hinge is restricted by low deployment moment or efficiency. To tackle this problem, more feasible approach of configurations [5–16], optimization of material properties [17–34] and advanced manufacturing technologies [35–52] should be performed to enhance the recovery ability. In case the tunable recovery moment of the intelligent hinge is realized, a bigger power will be achieved than we can image in deployable structures [53–72].

In recent years, the deployment performance of the intelligent hinge was investigated by several scholars. Kim et al. [73] proposed a tape spring intelligent hinge and then solved its nonlinear behavior problem in experimental ways. Picault et al. [74] shown the large change of in-plane cross-section shape of tape spring hinges, which used the experimental results and dynamic methods. Soykasap et al. [17] explored a new configuration of carbon fiber reinforced plastic by geometrically nonlinear finite element modeling. Kwok et al. [4] shown a viscoelastic polymer tape spring hinge. And they investigated the change of relaxation modulus, which was based on the effect of geometric nonlinear, time and temperature dependence. Leng et al. [75] provided a new prototype of intelligent hinge that can give a higher bending moment. Then they investigated the fundamental thermal and mechanical properties of intelligent materials by using differential scanning calorimetry, dynamic mechanical analysis, and tensile test [76]. Jeong et al. [77] proposed a novel design of tape spring hinge, which can maximize the deployment stiffness and torture. Ahn et al. [78,79] investigated a smart soft composite hinge actuator and introduced the manufacture of this hinge actuator. Then the maximum bending curvature was studied in experimental ways. Nevertheless, the low recovery efficiency of intelligent hinge still can never escape our attention, which restricts the application of intelligent hinge.

In this paper, based on a creative method, the mechanical design

---

* Corresponding author. Center for Composite Materials, Harbin Institute of Technology, Harbin 150001, PR China.
E-mail address: wangcg@hit.edu.cn (C. Wang).

of hybrid intelligent hinge system is proposed. This system is made up of two shape memory polymer (SMP) thin shells and one spring sheet, which enhancement of bending moment is expected by this configuration. The theoretic predictions of bending moment of intelligent hinge system are achieved by the theory of plates and shells. The large deformation simulations [80] of hybrid intelligent hinge system make it possible to divide the bending process into three typical stages. With bending stages different, the corresponding bending mechanisms are different. Verification of recovery ability of the hybrid intelligent hinge system is performed by experimental results. For bending rules to obtain, it is necessary to conduct the parametric analysis of the hybrid intelligent hinge system. Upon realizing the tunable recovery moment, the hybrid intelligent hinge will have a promising future in deployable structures.

2. Design and analysis of hybrid intelligent hinge

2.1. The concept of hybrid intelligent hinge

In this part, we develop a kind of hybrid intelligent hinge with thermosetting SMP and spring sheet, which is based on the win-win considerations. For one thing, intelligent hinge is only made up of pure SMPs, which its deployment time usually needs hundreds of seconds [4]. However, due to the outstanding properties, especially in aspect of self-lock and self-deployment, SMP intelligent materials have an advantage in deployable structures. For another, opposite to the gentle deployment behavior of the SMP hinge, large elastic strain energy will release instantly when spring sheet hinge has a large deformation. And this instant shock will probably cause a disaster, such as the disorder of the satellite system.

Fig. 1 illustrates a hybrid intelligent hinge system in its full deployable state, containing two SMP thin shells and one spring sheet, with two polyimide heaters as heating layers. With the support of heating layers, the reshaping of two SMP shells can be achieved by heating up to its glass transition temperature. Then the large elastic strain energy will not instant release because of self-adoptability of SMP. Independence of the hybrid intelligent hinge system can be achieved by simplifying the deployment form, which improves the deployment efficiency in deployable structures.
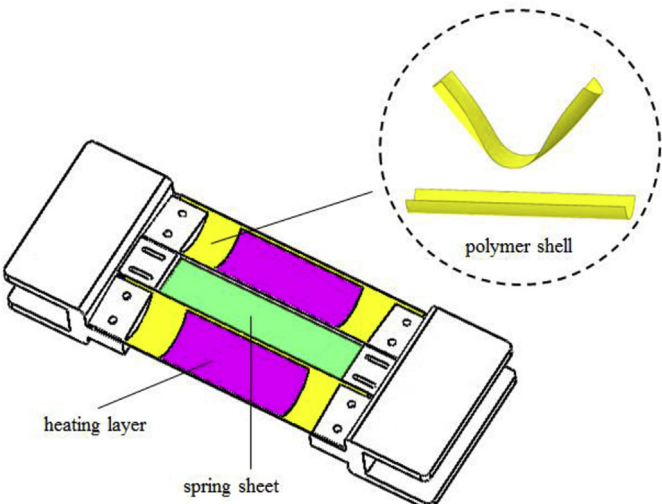

Fig. 1. The hybrid intelligent hinge system.

2.2. Bending moment of intelligent hinge

Polymer shells researched here are cylindrical shells, which its cross-sections have curvatures. Bending approaches of the SMP shell include opposite-sense bending and equal-sense bending. Generally, the cylindrical shell will have a higher sectional moment of inertia when compared with the plate structure. Thus, a larger bending stiffness can be achieved by this sectional configuration. Fig. 2 is the model of polymer shell. According to the theory of plates and shells, the bending moments are

$$M_x = D(\kappa_x + v\kappa_y) \tag{1}$$

$$M_y = D(\kappa_y + v\kappa_x) \tag{2}$$

where κ_x and κ_y are curvatures in different directions, D is the bending moment of the polymer shell. When polymer shell is in the state of equal-sense bending, the changes of curvatures are

$$\left.\begin{array}{l} \kappa_x = 0 - \dfrac{1}{r} = -\dfrac{1}{r} \\[2mm] \kappa_y = \dfrac{1}{R} - 0 = \dfrac{1}{R} \end{array}\right\} \tag{3}$$

the elastic strain energy produced by larger deformation of polymer shell can be expressed as:

$$U = \frac{Rr\psi\theta}{2}(\kappa_x, \kappa_y)(M_x, M_y)^{\mathrm{T}} \tag{4}$$

then substituting Eqs. (1) to (3) into Eq. (4), according to principle of minimum potential energy, it is formulated as:

$$\frac{\partial U}{\partial r} = \frac{\psi\theta D}{2} \cdot \frac{\partial}{\partial r}\left(\frac{R}{r} + \frac{r}{R} - 2v\right) = 0 \tag{5}$$

next substituting the result $R = r$ into Eq. (1), which result in:

$$M_x = \frac{D}{R}(1 + v) \tag{6}$$

then integrating Eq. (6), the equal-sense bending moment can be written as:

$$M_p = \int_{s_0=0}^{s_1=\theta R} M_y ds = D\theta(-1 + v) \tag{7}$$

the same procedure could be adapted to opposite-sense bending moment:

$$M_n = \int_{s_0=0}^{s_1=\theta R} M_y ds = D\theta(-1 + v) \tag{8}$$

where bending stiffness is

$$D = \frac{Et^3}{12(1 - v^2)} \tag{9}$$

Eqs. (7) and (8) indicate that bending moments have no relationship with the length and sectional radius of a polymer shell. And a linear dependence is found between bending moment and shell sectional angle, when shell thickness stays a constant. In response to this, if shell sectional angle is a constant, there is a
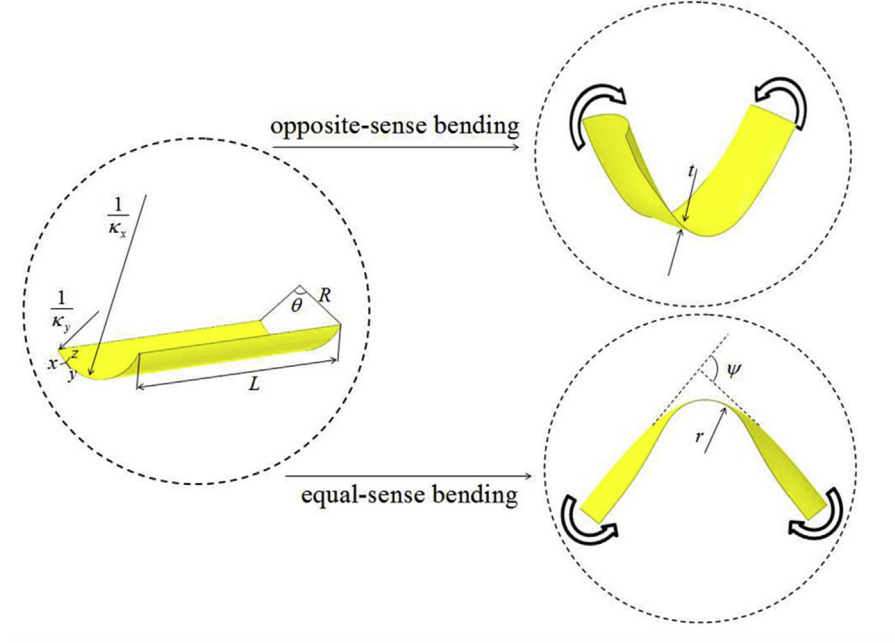
Fig. 2. The model of SMP shell.

power function relationship between bending moment and shell thickness.

On the other hand, in the $\alpha - \beta - \gamma$ orthogonal curvilinear coordinate system, due to pure bending state of the polymer shell, membrane internal force and torque of unit width in the middle surface are equal to zero. Hence, according to the internal equations of shell, we obtain following equations:

$$\left. \begin{array}{l} F_{T1} = \dfrac{Et}{1-v^2}(\varepsilon_1 + v\varepsilon_2) = 0 \\[2mm] F_{T2} = \dfrac{Et}{1-v^2}(\varepsilon_2 + v\varepsilon_1) = 0 \\[2mm] F_{T12} = F_{T21}\dfrac{Et}{2(1+v)}\varepsilon_{12} = 0 \\[2mm] M_{12} = M_{21} = (1-v)D\chi_{12} = 0 \end{array} \right\} \quad (10)$$

where F_{T1}, F_{T12} are unit width tension (or pressure), shear force applied in α plane. F_{T2}, F_{T21} are counterparts in β plane. ε_1, ε_2 are linear strain in α, β direction and ε_{12}, χ_{12} are shear strain, torsional curvature in both planes. Therefor

$$\varepsilon_1 = \varepsilon_2 = \varepsilon_{12} = \chi_{12} = 0 \quad (11)$$

without considering the influence of σ_3 on the deformation of polymer shell, by using physical equations, we can obtain the equations:

$$\left. \begin{array}{l} \sigma_1 = \dfrac{E}{1-v^2}[(\varepsilon_1 + v\varepsilon_2) + (\chi_1 + v\chi_2)\gamma_h] \\[2mm] \sigma_2 = \dfrac{E}{1-v^2}[(\varepsilon_2 + v\varepsilon_1) + (\chi_2 + v\chi_1)\gamma_h] \\[2mm] \sigma_3 = 0 \\[2mm] \tau_{12} = \dfrac{E}{2(1+v)}(\varepsilon_{12} + 2\chi_{12}\gamma_h) \end{array} \right\} \quad (12)$$

where σ_1, σ_2, τ_{12} are normal stress and shear stress in α, β direction,

χ_1, χ_2 are changes of principle curvature in α, β direction, γ_h represents the distance that surface is parallel to the middle surface. Then substituting Eqs. (3) and (11) into Eq. (12), the stresses can be expressed as:

$$\left. \begin{array}{l} \sigma_1 = \dfrac{E\gamma_h}{1-v^2}(\chi_1 + v\chi_2) = \dfrac{E\gamma_h}{R(1-v^2)}(1-v) \\[2mm] \sigma_2 = \dfrac{E\gamma_h}{1-v^2}(\chi_2 + v\chi_1) = \dfrac{E\gamma_h}{R(1-v^2)}(v-1) \\[2mm] \sigma_3 = 0 \\[2mm] \tau_{12} = 0 \end{array} \right\} \quad (13)$$

In addition, by using the results $\sigma_1 = -\sigma_2$ and $\gamma_h = t/2$, and then according to the Mises Criterion:

$$(\sigma_1 - \sigma_2)^2 + (\sigma_2 - \sigma_3)^2 + (\sigma_3 - \sigma_1)^2 \leq 2\sigma_s^2 \quad (14)$$

the ratio range of t/R can be given by:

$$\frac{t}{R} \leq \frac{2\sqrt{3}(1+v)\sigma_s}{3E} \quad (15)$$

Based on the analysis of polymer shell, bending moment of the spring sheet is easy to deduce by analogous method, utilizing Eq. (1) and the changes of curvatures $\kappa_x = -1/r$, $\kappa_y = 0$, the bending moment can be expressed as:

$$M_s = \int_0^a \left(-\frac{D_s}{r_s} \right) dy = -\frac{Et_s^3 a_s}{12 r_s (1 - v_s^2)} \quad (16)$$

where parameters of the spring sheet refer to that of polymer shell, and the subscript s accordingly indicates the spring sheet. As for the bending moment of the intelligent hinge system that should include three separate parts. Linear superposition of bending moment can be applied to two polymer shells, and a correlation coefficient should be added when considering the function of a

spring sheet

$$M = \eta M_p + \xi M_s \qquad (17)$$

where η is the number of polymer shells, ξ is the correlation coefficient that can be obtained by simulations or experimental results.

2.3. Bending behaviors of intelligent hinge

The bending behaviors of the single polymer shell, spring sheet, two polymer shells and hybrid intelligent hinge system are obtained and compared in Fig. 3. The whole bending process can be divided into three typical stages: the stage I of initial linear bending, the stage II of energy loss and stage III of deforming resistance of spring sheet. These three typical stages correspond with three bending mechanisms. In stage I of initial linear bending, Fig. 3(a) indicates that increasing moment of hybrid intelligent hinge system is mainly produced by two polymer shells. Spring sheet is not functional in such a slight rotation. In stage II of energy loss, a change of relative displacement of shell cross-section can explain the reason why the moment-rotation curve has a sharp decline in Fig. 3(a). Relative displacements of two shells cross-sections are

convex shapes originally in stage II. However, due to a slight increasing of rotation, the cross-sections are transformed from convex shapes to concave shapes. The mutation of sectional shape can induce a large energy loss, based on which the dramatic decrease of bending moment can be found in Fig. 3(a). The reinforcement of spring sheet is gradually appearing in stage II, which explains the reason of fluctuation in decline process. In stage III of deforming resistance of spring sheet, dominant status of spring sheet can be accomplished by a relative large rotation. Deforming resistance of spring sheet can give a moderate moment increasing of hybrid intelligent hinge in the bending process. Moreover, dominant status of spring sheet will become more and more apparent, until submerging the energy loss process because of two polymer shells. Finally, the bending tendency of hybrid intelligent hinge will be similar to spring steel counterpart without any large energy loss.

According to Fig. 3(b), the bending moment of spring sheet has an upward tendency. Not like the linear increasing, sharp increase of the single polymer can be found initially in curve. And then the curve reaches a peak in 13.7°, after this, with the dramatic decline, a
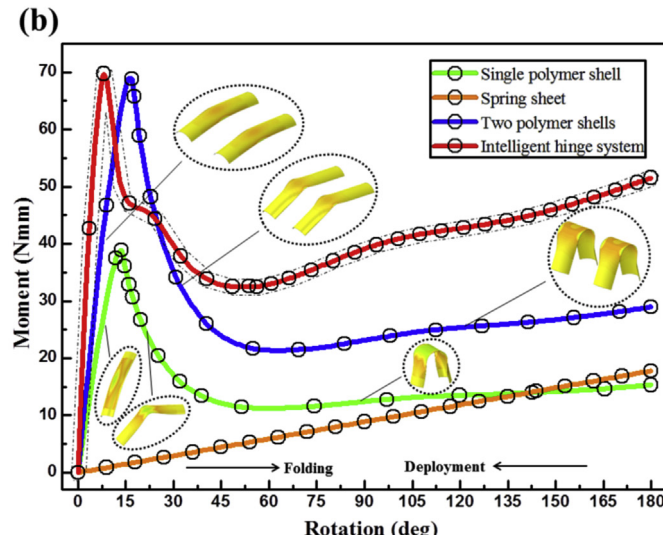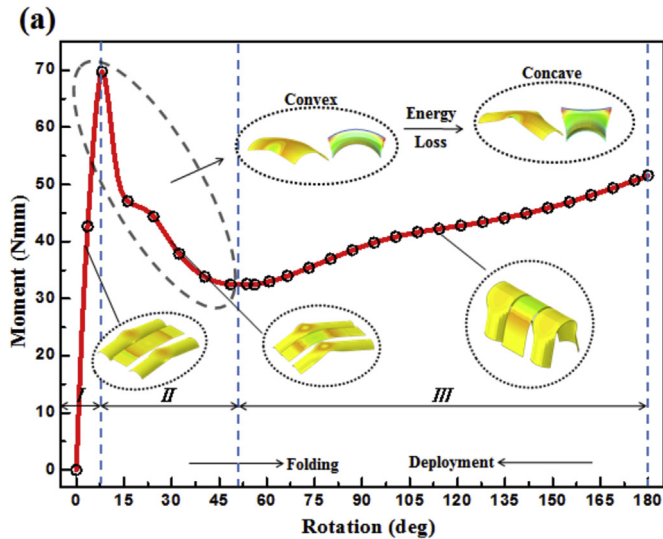

**Fig. 3.** The bending behaviors of hybrid intelligent hinge system.
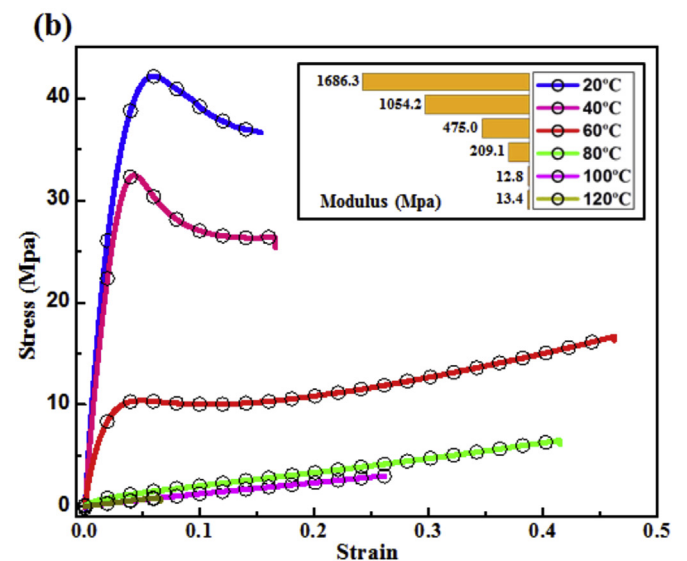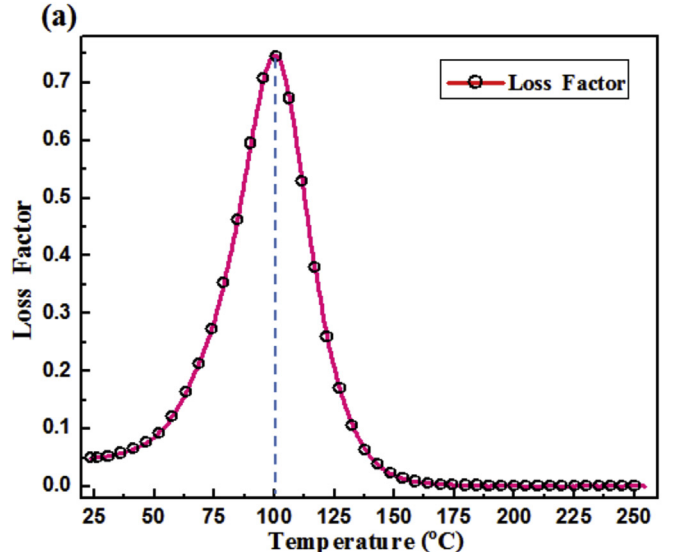
**Fig. 4.** Mechanical Testing of SMP. (a) Dynamic mechanical analysis. (b) Tensile testing.
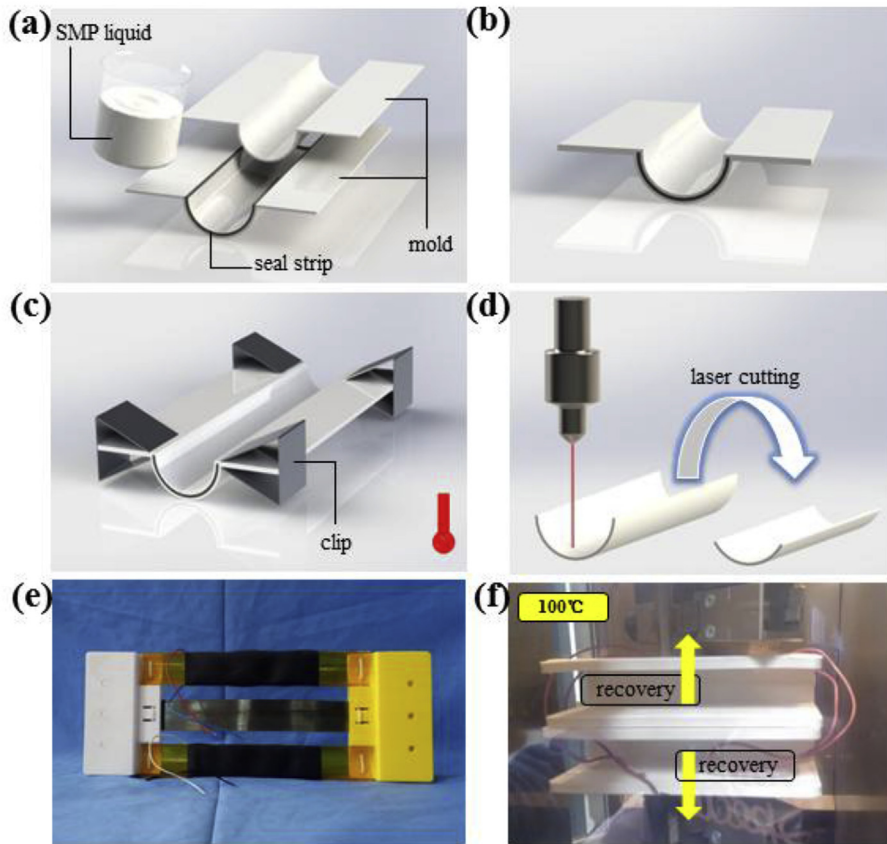
Fig. 5. Fabrication and experiment of hybrid intelligent hinge. (a) To (d) fabrication processes of SMP shell. (e) Specimen of hybrid intelligent hinge. (f) Deployable moment testing.
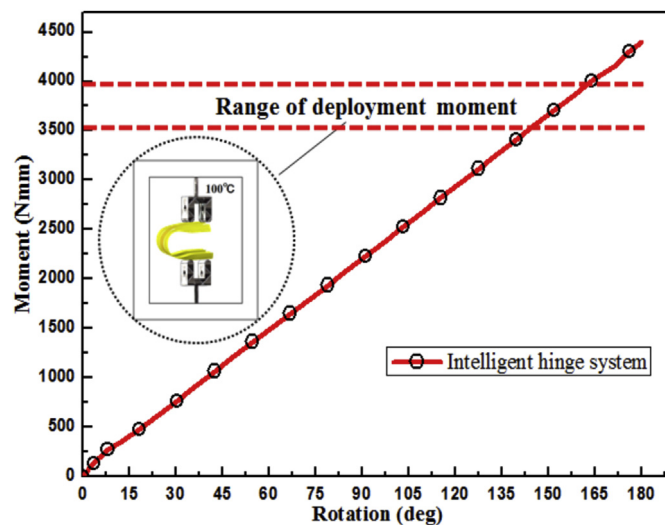

Fig. 6. Experimental data of deployment moment (thickness of spring sheet is 0.6 mm).

period of gradual increase can be discovered. Similarly, intelligent hinge made up of two polymer shells has a significant increase trend, growing from 0° to 16.9°. Then the curve decreases abruptly and reaches the bottom at 62.1°. Finally, bending moment has a modest increase from 62.1° to 180°. In conclusion, enhancement of bending moment can be achieved by adding the number of shells. And the predominating function of spring sheet can be found in

both folding and deployment processes. Meanwhile, through comparing the bending behaviors of different shells numbers, we find two polymer shells reaching the highest point is later than that of a single shell in Fig. 3(b). This indicates that the energy loss of bending process of intelligent hinge can be postponed by multiple polymer shells. However, the corresponding highest point of hybrid intelligent hinge system is earlier than others. This is because, due to adding the spring sheet, configuration approach of hybrid intelligent hinge makes it possible to transfer stress more quickly from end region of hybrid intelligent hinge to middle region. And this special bending mechanism induces the instability of hybrid intelligent hinge system initially.

2.4. Experimental verifications of intelligent hinge recovery ability

In order to explore the recovery ability and to demonstrate an application potential of the intelligent hinge, the fundamental mechanical performance testing of SMP should be conducted firstly. In dynamic mechanical analysis, as shown in Fig. 4(a), glass transition temperature is defined as peak value of the loss factor, the value is 100 °C. In contrast, statics mechanical testing or tensile testing in Fig. 4(b) indicates that elastic modulus will decrease along with the temperature increasing. And the minimum value of elastic modulus is also the glass transition temperature. In addition, the fabrication processes of SMP shell is shown in Fig. 5. Firstly, the uncured SMP liquid is poured into mold with the silicone rubber seal strips (as shown in Fig. 5(a) and (b)). Next, the fixture system with uncured SMP liquid is put into the oven for curing at 150 °C for 5 h (as shown in Fig. 5(c)). Finally, the available SMP shell is formed by laser cutting (as shown in Fig. 5(d)). As for the hybrid intelligent
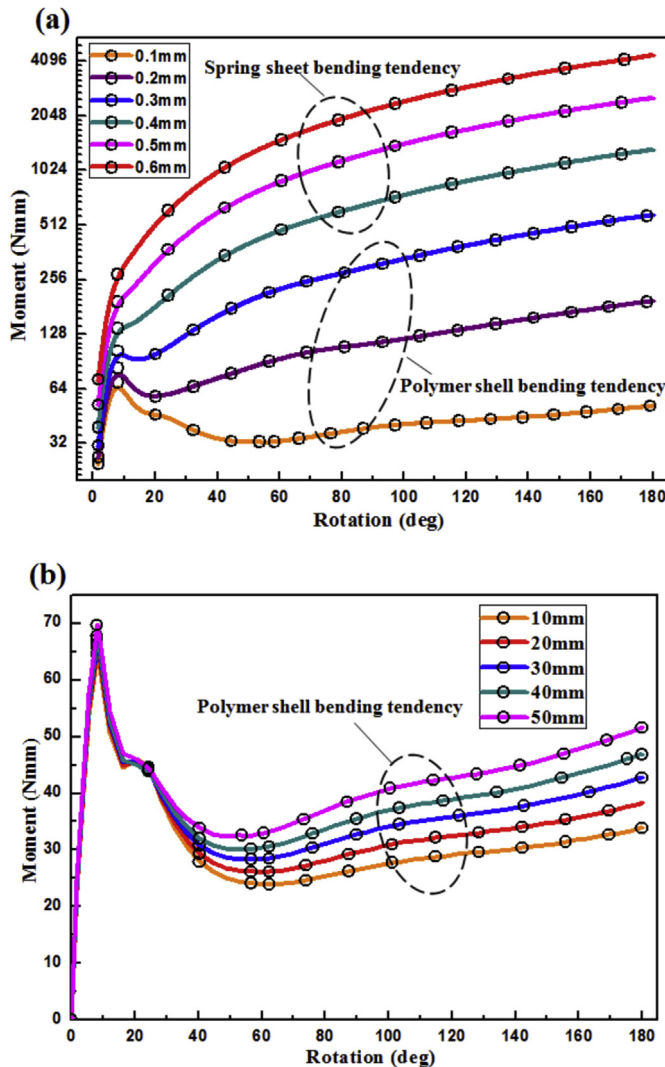
Fig. 7. The influence of spring steel parameter on recovery ability of intelligent hinge.

hinge, using the same methods, another SMP shell can be fabricated. By introducing the spring sheet (as seen in Fig. 5(e)), an available hybrid intelligent hinge can be achieved. Then recovery ability of intelligent hinge can be verified by experimental results and simulations. Based on shape memory effect of SMP, in the atmosphere of glass transition temperature, the hybrid intelligent hinge system will exert a recovery moment on outside restraint (as shown in Fig. 5(f)). Hence, deployment moment of hybrid intelligent hinge can be achieved by using electronic tensile tester with the temperature box. As seen in Fig. 6, the range of deployment moment is from 3500Nmm to 4000Nmm when outside constant temperature is 100 °C. Moreover, not like the pure SMP intelligent hinge, its deployment time usually needs hundreds of seconds [4]. The deployment testing is carried out to demonstrate the excellent recovery ability of hybrid intelligent hinge system, and the deployment time is about 80s. In conclusion, the enhancement of recovery ability can be achieved by the hybrid intelligent hinge system with SMP shells and spring sheet.

2.5. Parametric analysis of intelligent hinge

In numerical simulations, by creating the 3D shell models, simulation models of polymer shells and spring sheet can be established in ABAQUS. And the geometric nonlinearity should be opened in simulations process. By exerting the rotation angle at each end of hinge, the nonlinearity large deformation of hybrid intelligent hinge system can be realized. As for two polymer shells, Eq. (7) indicates that the bending moment has no relationship with the length and sectional radius of the polymer shells. The linear dependence and power function relationships can be found in relative parameters. Hence, based on the simulations and theoretic derivations, the thickness and sectional angle of polymer shells are set as 2mm and 120°. As for spring sheet, Eq. (16) indicates that the bending moment has a power function relationship with thickness of spring sheet, and a linear dependence with sectional span length of spring sheet. Based on simulations and experimental results, by comparing material properties of SMP and spring sheet, the bending moment of hybrid intelligent hinge system is mainly depended on thickness and sectional span length of spring sheet. Considering the dominant status of spring sheet in bending process, the parametric analysis of hybrid intelligent hinge system can be illustrated in Fig. 7.

As shown in Fig. 7(a), the thickness of spring sheet has a great influence on recovery ability of hybrid intelligent hinge. With the thickness increasing, recovery moment is increased accordingly. In Fig. 7(a), the thickness of spring sheet is increased from 0.1 mm to 0.6 mm, which the mass of spring sheet is increased by six times. However, the recovery moment of hybrid intelligent hinge from 51.56 N to 4394 N is increased by 85 times. Therefore, with the spring sheet thickness slight increasing, recovery ability of hybrid intelligent hinge has a great enhancement. Two bending tendencies can be found in Fig. 7, which are spring sheet bending tendency and polymer shell bending tendency. In this paper, we refer to the dominant status of spring sheet which will become more and more apparent. Just as the change of bending tendency in Fig. 7(a), with the thickness increasing, energy loss because of two polymer shells is submerged by dominant status of spring sheet. Hence, by choosing the proper thickness of spring sheet, we can achieve a special hybrid intelligent hinge, with the great enhancement of recovery efficiency, without any large energy loss. Hybrid intelligent hinge with 0.6 mm thickness spring steel will be selected here. According to Fig. 7(b), due to the linear relationship between sectional span length and bending moment, increasing of sectional span length will not change a polymer shell bending tendency. In addition, considering assembly relationship of the hybrid intelligent hinge, we use the projected span length of the polymer shell as the sectional span length of spring sheet. In conclusion, through performing the parametric analysis of hybrid intelligent hinge, the bending rules of hybrid intelligent hinge system can be achieved. And the hybrid intelligent hinge system with a variable range of recovery moment can be designed.

The single use of hybrid intelligent hinge is not the final aim in this research, which series or parallel or hybrid use will develop the application scope. Through the combined use of multiple hybrid intelligent hinges, a controlling nonlinearity intelligent hinge tunable system will be achieved. Meanwhile, based on the parametric analysis of hybrid intelligent hinge, a variable range of recovery moment makes it possible to design a promising intelligent hinge of deployable structures.

3. Conclusion

A hybrid intelligent hinge with two shape memory polymer thin shells and one spring sheet is investigated in this paper. Then analyses of bending behaviors are carried out to guide the parametric design of hybrid intelligent hinge. And the dominant status of spring sheet can be found in the whole bending process. The main conclusion can be illustrated in terms of the following points.

Firstly, the whole bending process of hybrid intelligent hinge can be divided into three typical stages: the stage I of initial linear bending, the stage II of energy loss and stage III of deforming resistance of spring sheet. The relative displacements of shell cross-sections are changed from convex shapes originally to concave shapes in stage II. And due to this mutation of sectional shape transition, the large energy loss induces the dramatic decrease of bending moment. Secondly, through the parametric analysis of hybrid intelligent hinge, the bending rules of hybrid intelligent hinge system can be obtained. Recovery ability of hybrid intelligent hinge is very sensitive to the thickness of the spring sheet. Finally, based on the mechanical design of the hybrid intelligent hinge, a variable range of recovery moment will make it possible the combined use of multiple hybrid intelligent hinges. And a promising application of this hybrid intelligent hinge will be achieved by the obtained results in this paper.

Acknowledgements

References

[1] Beavers FL, Munshi NA, Lake MS, et al. Design and testing of an elastic memory composite deployment hinge for spacecraft applications. In: Proceedings of 43th AIAA/ASME/ASCE/AHS/ASC structures, structural dynamics, and materials conference. Denver, Colorado: AIAA -2000-1452; April 2002. p. 22–5.

[2] Zuckermandel J, Enger S, Gupta N. Design, build, and testing of TacSat thin film solar arrays. In: Proceedings of 4th international energy conversion engineering conference and exhibit (IECEC). San Diego, California: AIAA-2006-4198; June 2006. p. 26–9.

[3] Barrett R, Taylor R, Keller P, et al. Design of a solar array to meet the standard bus specification for operation responsive space. In: Proceedings of 48th AIAA/ASME/ASCE/AHS/ASC structures, structural dynamics, and materials conference. Honolulu, Hawaii: AIAA-2007-2332; April 2007. p. 23–6.

[4] Kwok K, Pellegrino S. Folding, stowage, and deployment of viscoelastic tape springs. AIAA J 2015;51(51):1908–18.

[5] Soykasap O. Folding design of composite structures. Compos Struct 2007;79(2):280–7.

[6] Yee JC, Pellegrino S. Composite tube hinges. J Aerosp Eng 2005;18(4):224–31.

[7] Soykasap O. Analysis of tape spring hinges. Int J Mech Sci 2007;49(7):853–60.

[8] Wang W, Rodrigue H, Ahn SH. Smart soft composite actuator with shape retention capability using embedded fusible alloy structures. Compos Part B Eng 2015;78:507–14.

[9] Rodrigue H, Wang W, Bhandari B, et al. Cross-shaped twisting structure using SMA-based smart soft composite. Int J Precis Eng Manufacturing-Green Technol 2014;1(2):153–6.

[10] Zhang Z, Wu H, He X, et al. The bistable behaviors of carbon-fiber/epoxy antisymmetric composite shells. Compos Part B Eng 2013;47(3):190–9.

[11] Bodaghi M, Damanpack AR, Aghdam MM, et al. Active shape/stress control of shape memory alloy laminated beams. Compos Part B Eng 2014;56(1):889–99.

[12] Song SH, Lee H, Lee JG, et al. Design and analysis of a smart soft composite structure for various modes of actuation. Compos Part B Eng 2016;95:155–65.

[13] Kim HI, Han MW, Song SH, et al. Soft morphing hand driven by SMA tendon wire. Compos Part B Eng 2016;105:138–48.

[14] Chen F, Liu L, Lan X, et al. The study on the morphing composite propeller for marine vehicle. Part I: design and numerical analysis. Compos Struct 2017;168:746–57.

[15] Shim JE, Quan YJ, Wang W, et al. A smart soft actuator using a single shape memory alloy for twisting actuation. Smart Mater Struct 2015;24(12):125033.

[16] Zhakypov Z, Huang JL, Paik J. A novel torsional shape memory alloy actuator: modeling, characterization, and control. IEEE Robotics Automation Mag 2016;23(3):65–74.

[17] Yee JCH, Soykasap O, Pellegrino S. Carbon fibre reinforced plastic tape springs. In: Proceedings of 45th AIAA/ASME/ASCE/AHS/ASC structures, structural dynamics, and materials conference. Palm Springs, California: AIAA-2004-1819; April 2004. p. 19–22.

[18] Behl M, Razzaq MY, Lendlein A. Multifunctional shape-memory polymers. Adv Mater 2010;22(31):3388–410.

[19] Felton SM, Tolley MT, Shin BH, et al. Self-folding with shape memory composites. Soft Matter 2013;9(32):7688–94.

[20] Yao Y, Zhou T, Yang C, et al. Preparation and characterization of shape memory composite foams with interpenetrating polymer networks. Smart Mater Struct 2016;25(3):035002.

[21] Yao Y, Zhou T, Wang J, et al. 'Two way' shape memory composites based on electroactive polymer and thermoplastic membrane. Compos Part A Appl Sci Manuf 2016;90:502–9.

[22] Dawood M, El-Tahan MW, Zheng B. Bond behavior of superelastic shape memory alloys to carbon fiber reinforced polymer composites. Compos Part B Eng 2015;77:238–47.

[23] Azzawi WA, Epaarachichi J, Isalm M, et al. Quantitative and qualitative analysis of mechanical behaviour and dimensional stability of styrene based shape memory composites. J Intelligent Material Syst Struct 2017. 1045389X1770521.

[24] Hu J, Zhu Y, Huang H, et al. Recent advances in shape-memory polymers: structure, mechanism, functionality, modeling and applications. Prog Polym Sci 2012;37(12):1720–63.

[25] Czél G, Jalalvand M, Wisnom MR. Design and characterisation of advanced pseudo-ductile unidirectional thin-ply carbon/epoxy–glass/epoxy hybrid composites. Compos Struct 2016;143:362–70.

[26] Alian AR, Dewapriya MAN, Meguid SA. Molecular dynamics study of the reinforcement effect of graphene in multilayered polymer nanocomposites. Mater Des 2017;124:47–57.

[27] Ladani RB, Wu S, Kinloch AJ, et al. Multifunctional properties of epoxy nanocomposites reinforced by aligned nanoscale carbon. Mater Des 2016;94:554–64.

[28] Kang J, Wang C, Li D, et al. Nanoscale crosslinking in thermoset polymers: a molecular dynamics study. Phys Chem Chem Phys 2015;17(25):16519–24.

[29] Jing Q, Liu Q, Li L, et al. Effect of graphene-oxide enhancement on large-deflection bending performance of thermoplastic polyurethane elastomer. Compos Part B Eng 2016;89(1):1–8.

[30] Guan Q, Yuan L, Zhang Y, et al. Improving the mechanical, thermal, dielectric and flame retardancy properties of cyanate ester with the encapsulated epoxy resin-penetrated aligned carbon nanotube bundle. Compos Part B Eng 2017;123:81–91.

[31] Bekas DG, Tsirka K, Baltzis D, et al. Self-healing materials: a review of advances in materials, evaluation, characterization and monitoring techniques. Compos Part B Eng 2016;87:92–119.

[32] Taherzadeh M, Baghani M, Baniassadi M, et al. Modeling and homogenization of shape memory polymer nanocomposites. Compos Part B Eng 2016;91:36–43.

[33] Yang Q, Li G. Spider-silk-like shape memory polymer fiber for vibration damping. Smart Mater Struct 2014;23(10):105032.

[34] Guo J, Wang Z, Tong L, et al. Effects of short carbon fibres and nanoparticles on mechanical, thermal and shape memory properties of SMP hybrid nanocomposites. Compos Part B Eng 2016;90:152–9.

[35] Wu J, Chao Y, Zhen D, et al. Multi-shape active composites by 3D printing of digital shape memory polymers. Sci Rep 2016;6:24224.

[36] Rodrigue H, Wei W, Bhandari B, et al. Fabrication of wrist-like SMA-based actuator by double smart soft composite casting. Smart Mater Struct 2015;24(12):125003.

[37] Wang X, Jiang M, Zhou Z, et al. 3D printing of polymer matrix composites: a review and prospective. Compos Part B Eng 2017;110:442–58.

[38] Tian X, Liu T, Yang C, et al. Interface and performance of 3D printed continuous carbon fiber reinforced PLA composites. Compos Part A Appl Sci Manuf 2016;88:198–205.

[39] Yuan G, Bai Y, Jia Z, et al. Enhancement of interfacial bonding strength of SMA smart composites by using mechanical indented method. Compos Part B Eng 2016;106:99–106.

[40] Díaz Lantada A, Adrián DBR, Chacón Tanarro E. Micro-vascular shape-memory polymer actuators with complex geometries obtained by laser stereolithography. Smart Mater Struct 2016;25(6):065018.

[41] Shin DG, Kim TH, Kim DE. Review of 4D printing materials and their properties. Int J Precis Eng Manufacturing-Green Technol 2017;4(3):349–57.

[42] Chung S, Song SE, Cho YT. Effective software solutions for 4D printing: a review and proposal. Int J Precis Eng Manufacturing-Green Technol 2017;4(3):359–71.

[43] Leist SK, Zhou J. Current status of 4D printing technology and the potential of light-reactive smart materials as 4D printable materials. Virtual & Phys Prototyp 2016;11(4):1–14.

[44] Ge Q, Dunn CK, Qi HJ, et al. Active origami by 4D printing. Smart Mater Struct 2014;23(9):094007.

[45] Deng D, Chen Y. Origami-based self-folding structure design and fabrication using projection based stereolithography. J Mech Des 2015;137(2):021701.

[46] Bodaghi M, Damanpack AR, Liao WH. Self-expanding/shrinking structures by 4D printing. Smart Mater Struct 2016;25(10).

[47] Yang Y, Chen Y, Wei Y, et al. 3D printing of shape memory polymer for functional part fabrication. Int J Adv Manuf Technol 2016;84(9):2079–95.

[48] Ding Z, Yuan C, Peng X, et al. Direct 4D printing via active composite materials. Sci Adv 2017;3(4).

[49] Bakarich Shannon E, Gorkin Robert, Naficy Sina, et al. 3D/4D printing hydrogel composites: a pathway to functional devices. MRS Adv 2016;1(8):521–6.

[50] Zarek M, Layani M, Cooperstein I, et al. 3D printing: 3D printing of shape memory polymers for flexible electronic devices. Adv Mater 2016;28(22).

4166—4166.

[51] Ying L, Shaw B, Dickey MD, et al. Sequential self-folding of polymer sheets. Sci Adv 2017;3(3):e1602417.

[52] Li J, Monaghan T, Nguyen TT, et al. Multifunctional metal matrix composites with embedded printed electrical materials fabricated by Ultrasonic Additive Manufacturing. Compos Part B Eng 2017;113:342—54.

[53] Seffen KA, Pellegrino S. Deployment dynamics of tape springs. Proc R Soc A Math Phys Eng Sci 1999;455(455):1003—48.

[54] Walker SJI, Aglietti GS. Experimental investigation of tape springs folded in three dimensions. AIAA J 2006;44(1):151—9.

[55] Tao Q, Wang C, Xue Z, et al. Wrinkling and collapse of mesh reinforced membrane inflated beam under bending. Acta Astronaut 2016;128:551—9.

[56] Seffen KA, You Z, Pellegrino S. Folding and deployment of curved tape springs. Int J Mech Sci 2000;42(10):2055—73.

[57] Ballard ZC, Gerbo EJ, Thrall AP, et al. Behavior of sandwich panels in a deployable structure. J Struct Eng 2016;142(10):04016073.

[58] Schenk M, Viquerat AD, Seffen KA, et al. Review of inflatable booms for deployable space structures: packing and rigidization. J Spacecr Rockets 2015;51(3):762—78.

[59] Thrall AP, Quaglia CP. Accordion shelters: a historical review of origami-like deployable shelters developed by the US military. Eng Struct 2014;59: 686—92.

[60] Martínez-Martín FJ, Thrall AP. Honeycomb core sandwich panels for origami-inspired deployable shelters: multi-objective optimization for minimum weight and maximum energy efficiency. Eng Struct 2014;69(9):158—67.

[61] Zhang Y, Yang D, Li S. An integrated control and structural design approach for mesh reflector deployable space antennas. Mechatronics 2016;35:71—81.

[62] Soykasap O, Pellegrino S, Howard P, et al. Folding large antenna tape spring. J Spacecr Rockets 2008;45(3):560—7.

[63] Araromi OA, Gavrilovich I, Shintake J, et al. Rollable multisegment dielectric elastomer minimum energy structures for a deployable microsatellite gripper. IEEE/ASME Trans Mechatronics 2014;20(1):438—46.

[64] Brancart S, Laet LD, Temmerman ND. Deployable textile hybrid structures: design and modelling of kinetic membrane-restrained bending-active structures. Procedia Eng 2016;155:195—204.

[65] Yan C, Feng H, Ma J, et al. Symmetric waterbomb origami. Proc Math Phys Eng Sci 2016;472(2190):20150846.

[66] Chen Y, You Z, Tarnai T. Threefold-symmetric Bricard linkages for deployable

structures. Int J Solids Struct 2005;42(8):2287—301.

[67] Nelson Todd G, Lang Robert J, Pehrson Nathan A, et al. Deployable mechanisms and structures via developable lamina emergent arrays. J Mech Robotics 2016;8(3).

[68] Yan Z, Zhang MF, Wang MJ, et al. Controlled mechanical buckling for origami-inspired construction of 3D microstructures in advanced materials. Adv Funct Mater 2016;26(16):2629—39.

[69] Liu X, Gattas JM, Chen Y. One-DOF superimposed rigid origami with multiple states. Sci Rep 2016;6:36883.

[70] Wang C, Du X, Wan Z. Numerical simulation of wrinkles in space inflatable membrane structures. J Spacecr Rockets 2012;43(5):1147—50.

[71] Neville RM, Chen J, Guo X, et al. A Kirigami shape memory polymer honeycomb concept for deployment. Smart Mater Struct 2017;26(5).

[72] Wang CG, Xia ZM, Tan HF. Initial shape design and stability analysis of rib for inflatable deployable reflector. AIAA J 2015;53(2):486—92.

[73] Kim KW, Park Y. Systematic design of tape spring hinges for solar array by optimization method considering deployment performances. Aerosp Sci Technol 2015;46:124—36.

[74] Picault E, Marone-Hitz P, Bourgeois S, Cochelin B, Guinot F. A planar rod model with flexible cross-section for the folding and the dynamic deployment of tape springs: improvements and comparisons with experiments. Int J Solids Struct 2014;51(18):3226—38.

[75] Lan X, Liu Y, Lv H, et al. Fiber reinforced shape-memory polymer composite and its application in deployable hinge in space. Smart Mater Struct 2009;18(2):1282—94.

[76] Leng J, Xie F, Wu X, et al. Effect of the radiation on the properties of epoxy-based shape memory polymers. J Intelligent Material Syst Struct 2013;25(10):1256—63.

[77] Jeong JW, Yoo YI, Shin DK, et al. A novel tape spring hinge mechanism for quasi-static deployment of a satellite deployable using shape memory alloy. Rev Sci Instrum 2014;85(2). 025001-025001-10.

[78] Wang W, Rodrigue H, Kim HI, et al. Soft composite hinge actuator and application to compliant robotic gripper. Compos Part B Eng 2016;98: 397—405.

[79] Wang W, Rodrigue H, Ahn SH. Deployable soft composite structures. Sci Rep 2016;6:20869.

[80] Soykasap O. Deployment analysis of a self-deployable composite boom. Compos Struct 2009;89(3):374—81.